Ann. For. Res. 63(1): 284-291, 2020
ISSN: 18448135, 20652445

ANNALS OF FOREST RESEARCH
www.e-afr.com

COMPARISON OF IMAGE PROCESSING TECHNIQUES FOR CLASSIFICATION OF RED BLOOD CELL STRUCTURES

Gayatri Mirajkar
Arvind Gavali College of Engineering, Satara, Maharashtra, India
gayatrimirajkar@gmail.com

Abstract

Investigation of blood smear is a significant symptomatic test utilized in the determination of a variety of sicknesses. The strategy for programmed conclusion of minute blood smear pictures by recognizing and isolating it to various classes of cells that are featured in the paper. Robotization of this cycle eventually limits the extent of potential illnesses saving a extensive measure of time. Recognizable proof of red platelets (RBCs) is completed/done by the framework utilizing unique procedures of picture handling activities like pre-handling, tasks for morphology, marking and extraction of highlights to ascertain shape and size of the RBCs. Morphological properties can give data in regards to state of the cell. By these activities and computations, RBCs are arranged. There are 2 phases in red cell arrangement process, first is the detachment of RBCs to typical and strange followed by strange cells grouping to three subclasses in view of the cell shape and construction. The point of this framework is to help pathologist by giving fast outcomes by examining the smear tests. The fix of these sicknesses is conceivable, when it is recognized at a previous stage.

KEY: Classification, Red Blood, Comparison, image processing, techniques, Classification, red blood cell, structures

Introduction

The primary piece of the resistant arrangement of human body is framed by RBC additionally named as erythrocytes. Haemoglobin is a biomolecule contained in blood, which gives red tone to it. Absence of typical RBC in the body brings about absence of oxygen. Morphological changes are seen in mature red cells, during the illness. [1]. Risk factors: A portion of the gamble factors may incorporate Family ancestry, Substance uncovered, Disease therapy, Radiation, Inborn condition like down syndrome.[2] The primary parts of blood are RBCs, White Platelets (WBCs), Platelets and Plasma. In light of surface, variety, size, also, morphology of core and cytoplasm, the cell can be separated. Individual with the infection, has unusual count of cells and requirements clinical help.[3] During long haul stockpiling of blood, the morphology of red platelets (RBCs) goes through a crumbling interaction wherein discocytes are changed into echinocytes and afterward into spherocytes [1]. The biochemical and biophysical changes in this cycle are named as RBC stockpiling sores [2]. Such changes are likewise identified in cell maturing [3], recommending a pertinence between RBC morphological changes and cell maturing [4]. During the time spent RBC maturing, the deformability of RBCs is debilitated, and the delicacy of RBCs is upgraded [5, 6], which might cause changes in RBC capability, prompting antagonistic clinical results like expanded postoperative contamination, profound vein apoplexy, and multiorgan

disappointment [7]. In this way, factual examination of the dissemination of RBC morphology is critical to assessing the nature of put away RBCs. In light of cell morphology examination, this RBC arrangement strategy can likewise give demonstrative data on blood sicknesses [8, 9].

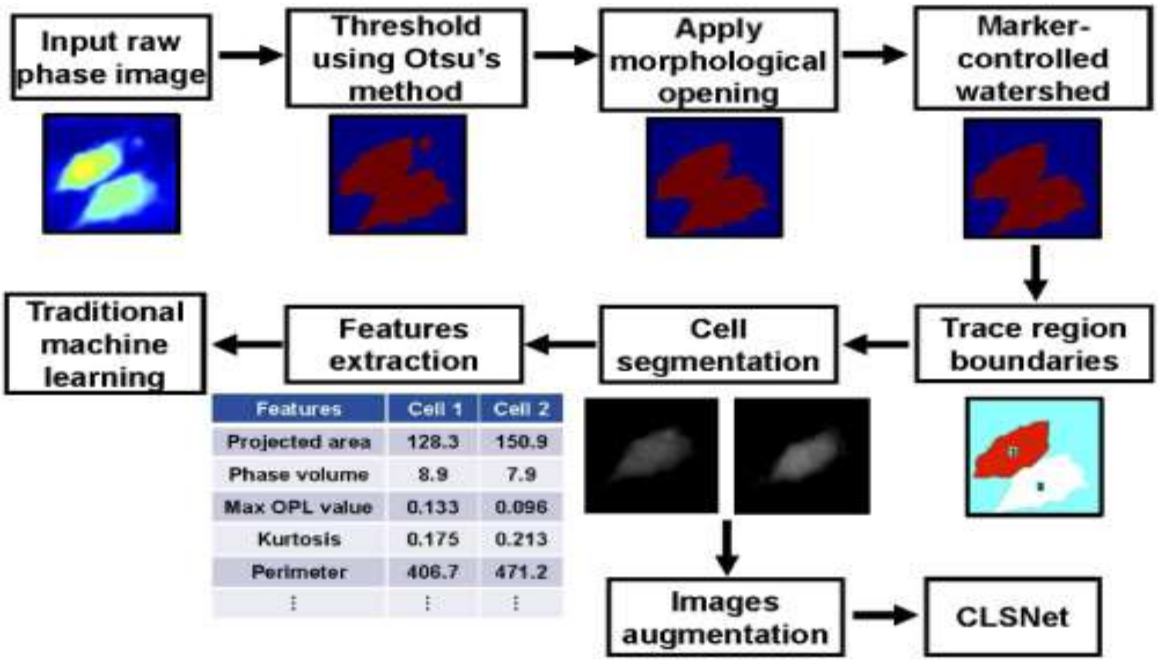

Fig.1: Comparison of image processing techniques for Classification of red blood cell structures flow.

With the improvement of code and man-made brainpower, the order calculations in light of AI [10-17] have empowered quick, effective, and programmed characterization of RBCs. Be that as it may, in most of past examinations, the extraction of morphological highlights of RBCs is physically screened, which is tedious and expects earlier information. In addition, most RBC programmed grouping strategies depend on conventional splendid field imaging advancements. In these imaging strategies, because of the little optical assimilation coefficient and unfortunate imaging differentiation of RBCs, the minute picture of clean RBCs isn't adequately clear to give an adequate number of subtleties to recognize among discocytes and splenocytes.

Materials and Methods

In [1], 1000 pictures were tested for determination. An exactness of 98% was distinguished accurately for sort of Iron deficiency which was assessed by the clinical Specialists/pathologists. In [3], cell counting relies upon legitimate acknowledgment of cell. The exactness of the pre-owned calculation relied upon the camera utilized, size of cells, whether cell contacting and light condition. In [5], the framework was just tried for two data sets, and may have various outcomes in various data sets. More properties of the created framework must be researched and ought to be tried on additional data sets. Be that as it may, data sets are troublesome to get. Prepared and

experienced master administrations are too expected to assess the nature of finding made by the framework.

Shows the flowchart of the mix of BC and SSAE to accomplish RBC grouping. In the first place, minute pictures were acquired by the stage reproduction technique in Area 2.1, and pictures with just single RBC were gotten by the division and extraction strategy in Next, the huge single-cell pictures were separated into three classifications of crude information x naturally as per the dataset arrangement strategy In the preparation stage, the different unique datasets x of RBCs, which were consequently partitioned into various grouping classifications (discocytes, echinocyte, and sphericity) by the order hyperplane, were input into SAE1 of SSAE to acquire the actuation esteem h1 and boundary W'. Also, h2, which was gotten by contributing h1 and W' into SAE2, was input into the Softmax classifier. To expand the precision of the model, x, h1, and h2 were reloaded into SSAE for calibrating [2][6] to limit L, the course of which was called as the profound brain organization (DNN). In the testing stage, BC in Area 2.5 was utilized to for starters screen the RBC stage pictures. After this screening, the pictures were input into the DNN to get the morphological elements of RBC.

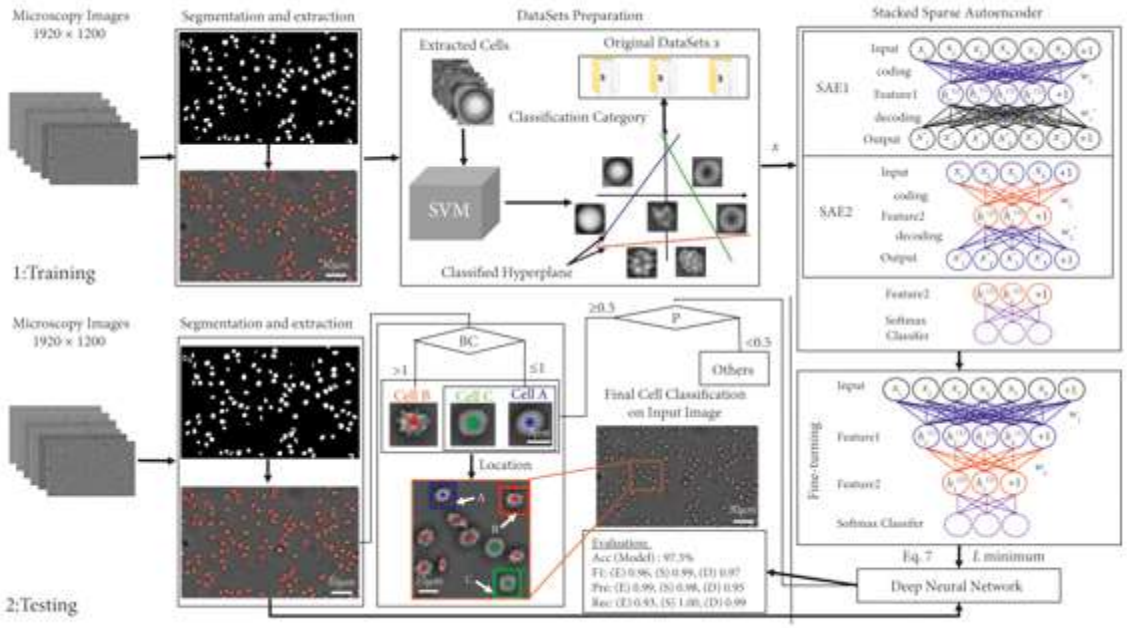

Fig.2: Comparison of image processing techniques for Classification of red blood cell structures process

RBC Sample

RBC tests were gathered from solid benefactors (matured 18-30 years). To comprehend the morphological changes of RBCs during capacity, a 5 ml entire blood test was gotten through the vein and put away in the CPDA-1 arrangement at the proportion of 1.4: 10, and afterward, the example was then saved in a cooler at 4°C ± 2°C. The morphology of RBCs was modified by changing the osmotic tension on phosphate support saline (PBS) [28]. For each example readiness, 10X PBS (Flash Jade, CR0015-500 ML, and China), 1X PBS (Flash Jade, CR0014-500 ML, China) with pH 7.1, and deionized water were blended to get a particular PBS with various osmotic tensions. The entire blood test was weakened with PBS at 1 : 100. The ruled morphologies of RBCs in hypertonic PBS (628 mOsm), isotonic PBS (300 mOsm), and hypotonic PBS (148 mOsm) are the echinocytes, discocytes, and spherocytes, separately. To acquire the three states of RBCs in similar picture, we mixed the blood put away for quite some time with new blood in isotonic PBS, where the natural temperature was kept at 22°C during the analysis.

RBC Segmentation

The preprocessing step of cell division is fundamental for RBC characterization, acknowledgment, and following [9, 3]. The associated area division calculation can without much of a stretch lead to mistaken division because of cell grip [3] [2]. The watershed division calculation in light of associated area examination is an expansion of the associated space division calculation [3], which can isolate the objective of halfway bond. To start with, the pictures were preprocessed by dim handling and reciprocal separating [4] to lessen the impact of foundation clamor on cell division. Second, the preprocessed pictures were handled by versatile limit, enlargement, disintegration, and morphological separating, which could diminish the impact of no cell substances on division.

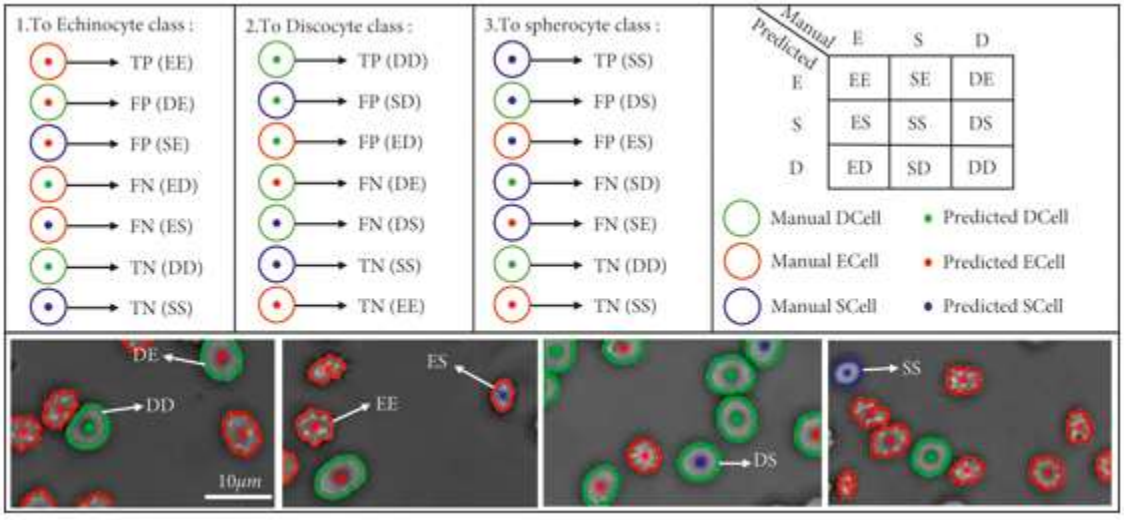

Fig.3: Red Blood Cell

Performance Metrics

From the assessment of the RBC grouping calculation, we commented on the genuine qualities with balanced circles of various varieties (red, green, and blue), which address the aftereffects of minuscule perception and RBC characterization by individual specialists. For quantitative assessment of the impact of our morphological characterization of RBCs, we took on the accompanying assessment plot, If the perception consequence of specialists is reliable with the calculation forecast outcome, it tends to be considered as a right expectation result (EE, SS, and DD), where the primary E in EE is the genuine worth and the subsequent E is the anticipated worth of our calculation.

Likewise, we can get SS and DD.(2)If the perception consequence of specialists is conflicting with the calculation forecast outcome, it tends to be considered as an off-base forecast outcome (SE, DE, ES, DS, ED, and SD), where E addresses the echinocyte, S addresses the spherocyte, and D addresses the discocyte. The upper left corner of Figure 4 shows the conceivable prescient aftereffects of the three states of RBCs, where green, red, and blue circles address the discocyte, echinocyte, and spherocyte identified physically, individually. Furthermore, green, red, and blue specks are the anticipated cell classifications for the RBCs.

Experimental Results

It is hard to notice the subtleties of impeccable RBCs by customary splendid field (BF) imaging innovation due to the unfortunate differentiation of straightforward and clear examples. To further develop the picture difference of RBC tests, we involved QPI innovation for tiny imaging of perfect RBCs. In the first place, as per the brightening points of the left and right 50% of Driven exhibits, two diagonal light pictures were caught by CCD, as displayed in Second, the left and right integral sideways brightening pictures were then changed into the left-right DPC picture (by condition (1). The top and base angled enlightenment pictures are displayed and the top-based DPC picture is displayed in similarly. At long last, QPI picture (was preestablished by DPC pictures utilizing stage move capability (condition (2)). To additionally imagine the three-layered design of QPI, lattice of RBC was determined by the cross section capability and view capability [48]. To all the more likely notice the two-layered design of the lattice picture, we set the azimuth and height to 0 and−88, separately.

Result

In view of the above boundary settings, the datasets of the three states of RBC were input into SSAE made out of a two-layer SAEs in addition to Softmax classifier for preparing by tweaking to frame the DNN. On the off chance that (condition (9)) was more prominent than 0.5, the expectation matching of the classification result was fruitful. Conversely, the expectations didn't

coordinate assuming the planning likelihood was under 0.5. Rehash the expectation multiple times for any RBC stage pictures as per the RBC order process displayed the last typical arrangement aftereffects of six RBC stage pictures, where E, S, and D are the echinocyte, spherocyte, and discocyte, individually.

Conclusions

In this review, we proposed a technique for programmed grouping of RBC morphology in light of QPI. In the first place, contrasted and the conventional brilliant field picture, QPI conveys better picture for examination of clean RBCs. Second, the watershed calculation in view of the associated space examination is utilized to show that QPI is more helpful for the division and acknowledgment of RBCs. Third, contrasted and the manual dataset, the dataset arrangement technique in view of SVM can keep away from the manual emotional mistake and subsequently increment the productivity. Last, the morphological highlights removed by BC and SSAE can be arranged by the Softmax classifier, and the misclassification pace of RBCs can be diminished by BC. The exploratory outcomes demonstrate the way that our grouping technique can accomplish programmed characterization of RBC morphology in light of QPI, with high precision, negligible estimation, quick acknowledgment speed, and no prerequisite to falsely set the component determination boundaries. What's more, our characterization strategy can possibly be applied to examination of RBC-related illnesses and assessment of the nature of long haul put away RBCs.

References

1) D. A. Sierra Fajardo, “Flow Cytomorphometry for Assessment of Red Blood Cell Storage Lesion,” Mannheim University, Mannheim, Germany, vol. 11, 2017.
2) J. F. Flatt, W. M. Bawazir, and L. J. Bruce, “The involvement of cation leaks in the storage lesion of red blood cells,” *Frontiers in physiology*, vol. 5, p. 214, 2014.
3) T. Kirkwood, “Cellular aging and cell death,” *British Journal of Cancer*, vol. 76, no. 1, p. 138, 1997.
4) I. Moon, F. Yi, Y. H. Lee, B. Javidi, D. Boss, and P. Marquet, “Automated quantitative analysis of 3D morphology and mean corpuscular hemoglobin in human red blood cells stored in different periods,” *Optics Express*, vol. 21, no. 25, pp. 30947–30957, 2013.
5) J. Yong, R. Ping, B. Feng, D. Endocrinology, and G. University, “The changes and clinical significance in morphological structure and membrane elasticity of red blood cells in T2DM patients,” *Chinese Journal of Diabetes*, vol. 21, pp. 998–1001, 2013.
6) Z. Xu, Y. Zheng, X. Wang, N. Shehata, C. Wang, and Y. Sun, “Stiffness increase of red blood cells during storage,” *Microsystems & Nanoengineering*, vol. 4, no. 1, Article ID 17103, 2018.
7) Whittle, M.; Quegan, S.; Uryu, Y.; Stüewe, M.; Yulianto, K. Detection of tropical deforestation using ALOS-PALSAR: A Sumatran case study. *Remote Sens. Environ.* **2021**, *124*, 83–98.

8) Van der Werf, G.R.; Morton, D.C.; DeFries, R.S.; Olivier, J.G.J.; Kasibhatla, P.S.; Jackson, R.B.; Collatz, G.J.; Randerson, J.T. CO_2 emissions from forest loss. *Nat. Geosci.* **2019**, *2*, 737–738.
9) Keenan, R.J.; Reams, G.A.; Achard, F.; de Freitas, J.V.; Grainger, A.; Lindquist, E. Dynamics of global forest area: Results from the FAO Global Forest Resources Assessment 2015. *For. Ecol. Manag.* **2020**, *352*, 9–20.
10) Le Quéré, C.; Andrew, R.M.; Friedlingstein, P.; Sitch, S.; Pongratz, J.; Manning, A.C.; Korsbakken, J.I.; Peters, G.P.; Canadell, J.G.; Jackson, R.B.; et al. Global Carbon Budget 2017. *Earth Syst. Sci. Data* **2018**, *10*, 405–448. [
11) Achard, F.; Stibig, H.-J.; Eva, H.D.; Lindquist, E.J.; Bouvet, A.; Arino, O.; Mayaux, P. Estimating tropical deforestation from Earth observation data. *Carbon Manag.* **2010**, *1*, 271–287.
12) Hansen, M.C.; Potapov, P.V.; Moore, R.; Hancher, M.; Turubanova, S.A.; Tyukavina, A.; Thau, D.; Stehman, S.V.; Goetz, S.J.; Loveland, T.R.; et al. High-Resolution Global Maps of 21st-Century Forest Cover Change. *Science* **2013**, *342*, 850–853.
13) Souza, J.; Siqueira, J.V.; Sales, M.H.; Fonseca, A.V.; Ribeiro, J.G.; Numata, I.; Cochrane, M.A.; Barber, C.P.; Roberts, D.A.; Barlow, J. Ten-Year Landsat Classification of Deforestation and Forest Degradation in the Brazilian Amazon. *Remote Sens.* **2013**, *5*, 5493–5513.
14) Hansen, M.C.; Krylov, A.; Tyukavina, A.; Potapov, P.V.; Turubanova, S.; Zutta, B.; Ifo, S.; Margono, B.; Stolle, F.; Moore, R. Humid tropical forest disturbance alerts using Landsat data. *Environ. Res. Lett.* **2016**, *11*, 034008.
15) H. Yu, J. Guo, W. Huang, L. Fang, and J. Zhao, "A deep learning approach for deforestation detection using SAR data," Remote Sensing, vol. 13, no. 3, p. 530, 2021.
16) S. Li, Y. Li, Z. Jiang, C. Li, and Y. Song, "A deep learning-based method for deforestation detection using Sentinel-1 SAR data," Remote Sensing, vol. 13, no. 8, p. 1482, 2021.
17) D. Tuia, C. Persello, and L. Bruzzone, "Multitemporal SAR image classification using deep learning: A land cover change detection application," IEEE Transactions on Geoscience and Remote Sensing, vol. 55, no. 3, pp. 1329-1345, 2017.
18) P. Chen, Y. Liu, W. Wang, H. Guo, Y. Zhang, and Y. Zhang, "Detection of deforestation in tropical forests using convolutional neural networks," Remote Sensing, vol. 11, no. 22, p. 2666, 2019.
19) Y. Liu, P. Chen, W. Wang, H. Guo, Y. Zhang, and Y. Zhang, "Deep convolutional neural networks for detecting deforestation in tropical forests using multi-source remote sensing data," Remote Sensing, vol. 11, no. 16, p. 1906, 2019.
20) T. Gindele, B. Waske, and M. Franke, "Deep learning for land cover classification and object-based deforestation detection using dual-polarimetric SAR data," Remote Sensing, vol. 11, no. 17, p. 2039, 2019.

21) X. Geng, H. Wang, L. Sun, Y. Li, and Y. Li, "Deep learning-based method for detecting deforestation using multispectral remote sensing images," International Journal of Remote Sensing, vol. 42, no. 1, pp. 294-308, 2021.
22) C. Huang, W. Wei, H. Xie, Y. He, L. Sun, and J. Zhang, "A deep learning-based method for deforestation detection in the Amazon rainforest using Landsat imagery," Remote Sensing, vol. 13, no. 5, p. 860, 2021.
23) W. Wei, H. Xie, C. Huang, Y. He, L. Sun, and J. Zhang, "Monitoring deforestation in the Amazon rainforest using deep learning and Landsat imagery," International Journal of Applied Earth Observation and Geoinformation, vol. 102, p. 102274, 2021.
24) M. H. Khan, S. S. Sultana, M. S. Rahman, and M. R. Islam, "A deep learning approach for deforestation detection using Sentinel-1 SAR data," ISPRS International Journal of Geo-Information, vol. 9, no. 7, p. 441, 2020.